

1 A Multiple 1D Earth Approach (M1DEA) to account  
2 for lateral viscosity variations in solutions of the sea  
3 level equation: An application for glacial isostatic  
4 adjustment by Antarctic deglaciation

5 R. Hartmann<sup>a,\*</sup>, J. Ebbing<sup>a</sup>, C.P. Conrad<sup>b</sup>

6 <sup>a</sup>*Institute of Geoscience, Kiel University, Kiel, Germany*

7 <sup>b</sup>*Center for Earth Evolution and Dynamics (CEED), University of Oslo, Oslo, Norway*

---

8 **Abstract**

The pseudo-spectral form of the sea level equation (SLE) requires the approximation of a radially-symmetric visco-elastic Earth. Thus, the resulting predictions of sea level change (SLC) and glacial isostatic adjustment (GIA) often ignore lateral variations in the Earth structure. Here, we assess the capabilities of a Multiple 1D Earth Approach (M1DEA) applied to large-scale ice load components with different Earth structures to account for these variations. In this approach the total SLC and GIA responses result from the superposition of individual responses from each load component, each computed globally assuming locally-appropriate 1D Earth structures. We apply the M1DEA to three separate regions (East Antarctica, West Antarctica, and outside Antarctica) to analyze uplift rates for a range of Earth structures and different ice loads at various distances. We find that the uplift response is mostly sensitive to the local Earth structure, which supports the usefulness of the M1DEA. However, stresses transmitted across rheological boundaries (e.g., producing peripheral bulges) present challenges for the M1DEA, but can be minimized under two conditions: (1) If the considered time period of ice loading for each component is consistent with the relaxation time of the local Earth structure. (2) If the load components can be subdivided according to the scale of the lateral variations in Earth structure. Overall, our results indicate that M1DEA could be a computationally much cheaper alternative to 3D finite element models, but further work is needed to quantify the relative accuracy of both methods for different resolutions, loads, and Earth structure variations.

9 *Keywords:* sea level change, uplift rates, GIA modeling, 3D Earth rheology,  
10 Antarctic ice loss, elastic lithosphere, upper mantle viscosities, rotational  
11 feedback, *SELEN*

---

\*Corresponding author

*Email address:* `r.hartmann@utwente.nl` (R. Hartmann)

## 12 1. Introduction

13 Accurate models of glacial isostatic adjustment (GIA) are essential for in-  
14 ferring present-day ice loss measurements and sea level changes from geodetic  
15 observations. It has been widely established that predicting sea level change  
16 (SLC) related to current and past melting events, and the associated GIA of  
17 the solid Earth, can be accomplished using the pseudo-spectral form of the  
18 sea level equation (SLE) (Mitrovica and Peltier, 1991), based on the sea level  
19 theory of Farrell and Clark (1976). Advanced formulations account for the feed-  
20 back of a rotating Earth (Milne and Mitrovica, 1998), grounding line migration,  
21 and shoreline migration (Milne et al., 1999; Kendall et al., 2005), all of which  
22 increase the accuracy of the predictions. But since the spectral solutions to  
23 the SLE require the approximation of a radially-symmetric visco-elastic Earth,  
24 these predictions cannot include lateral variations in Earth structure (e.g. Peltier  
25 et al., 2015; Martin-Español et al., 2016).

26  
27 Most regional models account for a 3D Earth structure by using a spatial  
28 form of the SLE in a finite element approach (Nield et al., 2018), which is com-  
29 putationally costly when applied on a global scale. A different approximation,  
30 recently used for GIA models of Greenland (Khan et al., 2016) and Antarc-  
31 tica (Sasgen et al., 2017, 2018), computes the GIA response to deglaciation  
32 in each regional basin separately, and sums the contributions. These individual  
33 GIA computations utilize different spherically-symmetric (1D) Earth structures,  
34 each chosen to be locally-appropriate for the basin that they represent. Their  
35 results suggest that such a Multiple 1D Earth Approach (M1DEA) can increase  
36 the accuracy of the predictions for SLC rates and GIA uplift rates compared to  
37 approaches based on a single 1D Earth structure. However, no detailed sensitiv-  
38 ity analysis for such an approach is yet available. Thus, it is still undetermined  
39 where the M1DEA improves GIA models with lateral variations in viscosity  
40 or where the neglected interaction of the individual Earth structures degrades  
41 such GIA models. For example, the long wavelength response to local loading  
42 or global effects like the rotational feedback (RFB) have not been characterized  
43 for M1DEA models.

44  
45 Antarctica provides an appropriate setup to analyze the capabilities of the  
46 M1DEA on large-scale load components, as East and West Antarctica differ  
47 geologically (e.g. Harley et al., 2013) and in their lithospheric (e.g. An et al.,  
48 2015) and viscosity structures (e.g. van der Wal et al., 2015).

49  
50 In this paper, we explore the impact of variations in Earth structure on local  
51 uplift rates for loads at various distances, with a focus on Antarctic deglaciation.  
52 Based on these results, we provide a preliminary assessment of the applicability  
53 of M1DEA to account for lateral variations in Earth’s rheology structure. While  
54 our results focus on the impact of lateral variations as implemented in M1DEA,  
55 our discussion uses their implications to motivate further investigations, espe-  
56 cially future tests between M1DEA and full 3D models.

57 **2. Multiple 1D Earth Approach (M1DEA)**

58 The redistribution of mass by surface loads affects the equipotential sea  
 59 surface (also defined as the Geoid) and the solid surface of the Earth. The local  
 60 difference of both displacements describes the SLC (e.g. [Mitrovica and Peltier,](#)  
 61 [1991](#); [Milne and Mitrovica, 1998](#)):

$$S(\vartheta, \varphi, t) = \mathcal{O}(\vartheta, \varphi, t) \cdot [N(\vartheta, \varphi, t) - U(\vartheta, \varphi, t)] \quad (1)$$

62 Here,  $N$  is the deformation of the geoid,  $U$  is the radial displacement of the  
 63 solid Earth, and  $S$  is the resulting SLC.  $\vartheta$ ,  $\varphi$ , and  $t$  denote longitude, latitude,  
 64 and time, respectively.  $\mathcal{O}$  is the ocean function ([Munk and MacDonald, 1960](#)),  
 65 which limits the sea level to oceanic regions.

66  
 67 In the pseudo-spectral form of the SLE the predicted deformations  $\Psi =$   
 68  $\{S, U, N\}$  and their corresponding rates  $\psi = \{s, u, n\} = \partial_t \Psi$  are linear to the  
 69 applied load  $L$ . Thus, total present-day rates are the superposition of all rates  
 70 induced by the different regional components of the ice load using the same  
 71 global 1D Earth model (Fig. 1(a)):

$$\psi_{\overline{\text{1D}}}(\vartheta, \varphi, t, \sum_{\text{reg}} L_{\text{reg}}) = \sum_{\text{reg}} \psi_{\overline{\text{1D}}}(\vartheta, \varphi, t, L_{\text{reg}}) \quad (2)$$

72 Here, the subscript reg indicates the various regional load components, which are  
 73 applied individually. The subscript  $\overline{\text{1D}}$  denotes the global 1D Earth structure.  
 74 In order to account for lateral variations, the Multiple 1D Earth Approach  
 75 (M1DEA) uses a specific regional 1D Earth structure  $\text{1D}_{\text{reg}}$  for each regional  
 76 load component (Fig. 1(b)):

$$\psi_{\text{M1DEA}}(\vartheta, \varphi, t, \sum_{\text{reg}} L_{\text{reg}}) = \sum_{\text{reg}} \psi_{\text{1D}_{\text{reg}}}(\vartheta, \varphi, t, L_{\text{reg}}) \quad (3)$$

77 In the M1DEA approximation, each 1D Earth structure is applied globally for  
 78 a given load, even though it may not be valid away from the regional load.  
 79 Hence, the combined rates at any point contain the contributions of multiple  
 80 relaxation behaviors from all Earth structures at that point. Our preinvestigation  
 81 (see App.: Fig. B.1) shows that the uplift rate in each region is mostly  
 82 dominated by the local loading and that the effect of loading in regions at great  
 83 distances is generally small. This implies that variations in the Earth struc-  
 84 ture of distant regions should have a minor effect as well (Fig. 1(c)). Aware  
 85 of the inherent inaccuracy of the M1DEA, we evaluate the capabilities of this  
 86 approach in this paper. The first step is to study the effect of large-scale varia-  
 87 tions between entire ice sheets, although the M1DEA can be used for small-scale  
 88 variations as well.

89

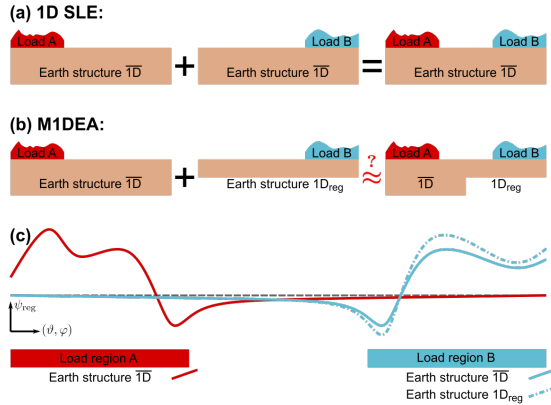


**Figure 1**

(a) "Standard" solution to the 1D SLE: A sketch of the superposition of load components A (red) and B (blue) each sitting above the same radially-symmetric average Earth structure  $\overline{1D}$  (Eq. 2), (b) Idea of the M1DEA: A sketch of the superposition of load components A (red) and B (blue) on different radially-symmetric Earth structures  $\overline{1D}$  and  $1D_{\text{reg}}$ , each describing the local structure beneath the load components A and B, respectively (Eq. 3), (c) Schematic rates (e.g., rates of uplift) induced by the load component A on the average Earth  $\overline{1D}$  (solid red line), the load component B on the average Earth  $\overline{1D}$  (solid blue line), and the load component B on the regional Earth  $1D_{\text{reg}}$  (dashed blue line). The M1DEA approximation works under the assumption that the induced rates are largest in the region of the corresponding load component (red and blue areas) and decrease outside this region. For the M1DEA, it is thus required that changes in the Earth structure beneath region B mostly only affect rates for region B, and not (much) for region A as well.

90 We calculate the various predictions of SLC  $S$ , ground surface displacement  
 91  $U$ , and sea surface displacement  $N$ , and their corresponding present-day rates  
 92  $\psi = \{s, u, n\}$ , using a modified version of *SELEN* 2.9.12 (Spada and Stocchi,  
 93 2007; Spada et al., 2012, 2015). This open source software package is based on  
 94 the pseudo-spectral SLE (Mitrovica and Peltier, 1991) for an incompressible,  
 95 non-rotating Earth with fixed shorelines. Further water expulsion is not consid-  
 96 ered. However, we have modified the code to consider the rotational feedback  
 97 (RFB) of the rotating Earth (Milne and Mitrovica, 1998; Mitrovica et al., 2001,  
 98 2005). Details on the implementation and the availability of the modified code  
 99 can be found in Appendix C. This is done to investigate the effect of the M1DEA  
 100 on global features like the RFB in addition to the local loading response. The  
 101 calculations truncate the SLE at spherical harmonic degree  $l_{\text{max}} = 128$ , which  
 102 gives a sufficient resolution for our aim - the assessment of the M1DEA for large-  
 103 scale variations in the Earth structure. All numerical parameters of *SELEN*,  
 104 which are used for all calculations, are summarized in Tab. A.1.

### 105 3. Test cases for the M1DEA

106 The SLE in *SELEN* basically depends on two physical quantities, the applied  
 107 load and a 1D visco-elastic structure of the Earth. Here, we briefly introduce

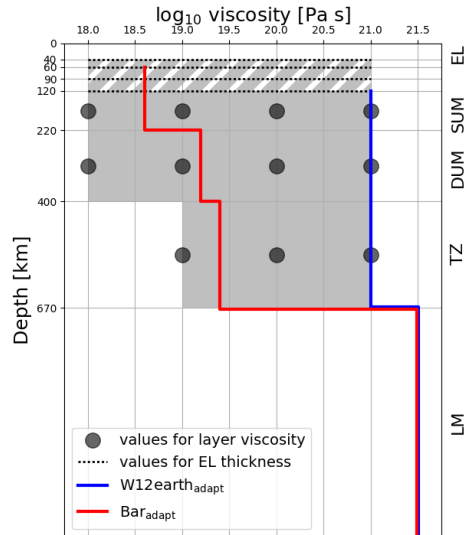


**Figure 2**

Applied viscosity profiles: The colored lines show the profiles for the specific tests applied. The dark gray dots represent the different considered values for the viscosities of the upper mantle layers in the sensitivity analysis. The covered range is shaded in lighter gray. The gray and white shaded portion illustrates the range that can be viscous or elastic depending on the chosen EL thickness. The explicit values for all Earth structures are summarized in Tab. A.3.

108 first the Earth structures and ice loading scenarios used for analysis of Earth  
 109 structure variations, and afterwards our sensitivity analysis itself.

### 110 3.1. Earth structures

111 All tests use an Earth structure with a general setting of six layers: the  
 112 core, the lower mantle (LM), the transition zone (TZ), the deep upper man-  
 113 tle (DUM), the shallow upper mantle (SUM), and the elastic lithosphere (EL)  
 114 (Tab. A.2). The Earth structure defines the density  $\rho$ , the shear modulus  $G$ ,  
 115 and the viscosity  $\mu$  of these layers, which are time-independent as *SELEN* as-  
 116 sumes an incompressible Earth and does not include stress-dependent terms.  
 117 The density and shear moduli within each layer are averaged values based on  
 118 the PREM model (Dziewonski and Anderson, 1981), and only the core is as-  
 119 sumed to be inviscid with a shear modulus set to  $G = 0$  and a viscosity of  $\mu = 0$ .  
 120 Furthermore, the basal depths of the mantle layers are fixed and the lithosphere  
 121 is treated as purely elastic.

122  
 123 Common 1D Earth structures for SLC or GIA predictions are the global  
 124 structure VM5a (Peltier and Drummond, 2008) and the optimum Earth model  
 125 of the W12 GIA model (Whitehouse et al., 2012b). These Earth structures  
 126 typically use viscosities around  $\mu = 10^{21}$  Pa s in the upper mantle and  $\mu \in$   
 127  $[10^{21.5}, 10^{22}]$  Pa s in the lower mantle. Such a relatively stiff Earth structure

128 is represented in our tests by the Earth structure  $W12_{\text{earth}}$  (Fig. 2, blue line).  
 129 Recent estimates predict very low viscosities in the upper mantle for several  
 130 regions of West Antarctica (Barletta et al., 2018; Zhao et al., 2017; Nield et al.,  
 131 2014). We follow the optimal model of Barletta et al. (2018) in the upper mantle  
 132 together with a lower mantle viscosity of  $\mu = 10^{21.5}$  Pa s (Fig. 2, red line) to  
 133 represent such a low-viscosity Earth structure.

134  
 135 Upper mantle viscosities vary across orders of magnitude. In order to de-  
 136 termine their impact on local uplift rates, we test 192 different combinations  
 137 over a large range of upper mantle viscosities and elastic thicknesses (Fig. 2:  
 138 gray zone, Tab. A.3). This allows for an individual analysis of viscosity and EL  
 139 variations.

### 140 3.2. Load components

141 The results shown are calculated using the long-term loading scenario ICE-  
 142 6G\_C (Argus et al., 2014; Peltier et al., 2015) (hereafter ICE-6G) subdivided into  
 143 several regional components. Since *SELEN* cannot account for shoreline and  
 144 grounding line migration, we corrected the total ice thicknesses of the ICE-6G  
 145 data for marine-grounded ice by the present-day bathymetry ETOPO (Amante  
 146 and Eakins, 2009) outside Antarctica and BEDMAP2 (Fretwell et al., 2013)  
 147 within the Antarctic region. The correction scheme is documented in Appendix  
 148 A (Eq. A.1, Fig. A.1, Tab. A.4).

#### 149 *Far-distant variations.*

150  
 151 We split ICE-6G at a latitude of  $60^\circ\text{S}$  into an Antarctic component ICE-6ant  
 152 and a Non-Antarctic component ICE-6far (Fig. 3). ICE-6far is then dominated  
 153 by the ice volume change in the northern hemisphere. These two components are  
 154 used to determine the impact of viscosity and EL variations at great distances  
 155 from the locations of predicted uplift.

#### 156 *Near-distant variations.*

157  
 158 The impact of the local variations of viscosity and EL are explored for neigh-  
 159 boring regions East and West Antarctica. Here, we additionally divide the  
 160 Antarctic component of the long-term scenario ICE-6G into an East Antarctic  
 161 component ICE-6eant and a West Antarctic component ICE-6want (Fig. 3). In  
 162 addition to the analysis for long-term loading (ICE-6G), we define the loading  
 163 scenarios  $WANT_{e1}$  and  $WANT_{100}$  to include the effect of present and most recent  
 164 ice loss in the sensitivity analysis. Therefore, we approximate the present-day  
 165 ice loss in West Antarctica with  $165 \frac{\text{Gt}}{\text{yr}}$  and a constant present-day ice balance  
 166 for East Antarctica ( $\pm 0 \frac{\text{Gt}}{\text{yr}}$ ), according to several estimates (Jacob et al., 2012;  
 167 The IMBIE team, 2018; Chen et al., 2009; Rignot et al., 2008). This corresponds  
 168 to an eustatic sea level change of  $\approx 0.46 \frac{\text{mm}}{\text{yr}}$ . The West Antarctic ice loss is  
 169 uniformly distributed over the present-day area of the West Antarctic region for  
 170 consistency with separation of the long-term components. The loading scenario

171 WANT<sub>100</sub> assumes a century of this rate of ice loss before present. The loading  
 172 scenario WANT<sub>el</sub> is a one-year scenario with melting at the present rate.

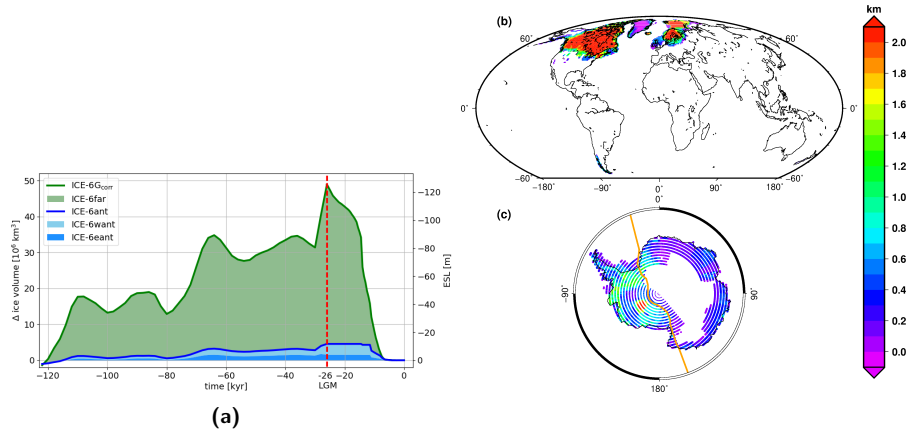


**Figure 3**

(a) Ice volume of the corrected loading scenario ICE-6G referenced to the present state (zero loading at  $t = 0$ ). The global volume (green line) is divided into the specific components (color shaded zones). The Antarctic component (blue line) consists of the East and West Antarctic components (blue shaded zones). The red line indicates the last glacial maximum (LGM). The right scale indicates the eustatic sea level (ESL) relative to the present state. (b) Ice extent at the LGM relative to the present state for the ICE-6far component. (c) Ice extent at the LGM relative to the present state for the ICE-6ant component. The orange line marks the border between the East and West Antarctic components.

### 173 3.3. Sensitivity analysis

174 We define the specific impact due to a particular Earth structure variation  
 175 beneath a given region of loading as following: Assume ice load in region  $B$   
 176 is modeled with an Earth structure  $v$ , and ice load in region  $A$  (outside  $B$ ) is  
 177 modeled with an Earth structure  $w$ . The impact caused by the varied structure  
 178  $v$  on the predicted rates  $\psi = \{s, u, n\}$  is the difference  $\Delta\psi$  between the predicted  
 179 M1DEA rates and the predictions using only Earth structure  $w$ :

$$\Delta\psi = \psi_{\text{M1DEA}} - \psi_{\text{homog}} = (\psi_{A,w} + \psi_{B,v}) - (\psi_{A,w} + \psi_{B,w}) = \psi_{B,v} - \psi_{B,w} \quad (4)$$

180 The (globally defined) difference  $\Delta\psi$  is expected to be large in region  $B$ , where  
 181 the M1DEA rates account for the varying structure  $v$ . However, the area of  
 182 interest is region  $A$ , where the M1DEA rates include the changed contribution  
 183 from load component  $B$  with Earth structure  $v$ . Small differences  $\Delta\psi$  in region  
 184  $A$  imply a low impact of the Earth structure  $v$  in region  $B$  on the rates in region  
 185  $A$ , which would indicate a good applicability for the M1DEA in this specific  
 186 combination.

187  
 188 Further, we can estimate a mean impact expected in region  $A$  due to any  
 189 variation of the Earth structure in region  $B$ , which is then simply the mean of

190 all tested specific impacts (Eq. 4):

$$\overline{\Delta\psi} = \frac{1}{N_{\text{mod}}} \sum_{v,w} |\psi_{B,v} - \psi_{B,w}| \quad (5)$$

191  $N_{\text{mod}}$  is then the number of combinations of Earth structures  $v$  and  $w$ . Both,  
 192 specific and mean impact, are given in absolute values of displacement rates  
 193 and of course have to be interpreted locally with respect to the predicted rates  
 194  $\psi(\vartheta, \varphi)$  at that point.

## 195 4. Results

196 Both SLC and GIA uplift rates contain an elastic contribution from present  
 197 loading and a viscous contribution from past loading. Here, we show the sensi-  
 198 tivity of these contributions to variations of the Earth structure - exemplary  
 199 for the uplift rates and GIA modeling.

### 200 4.1. Impact on the elastic contribution

201 We test the sensitivity of the elastic contribution by studying the elastic  
 202 response to uniform present-day Antarctic ice loss ( $\text{WANT}_{\text{el}}$ ). In the pseudo-  
 203 spectral SLE the elastic contribution is affected only by thickness, density, and  
 204 shear modulus of the EL. In our setup only EL thickness variations affect the  
 205 elastic contribution, since density and shear modulus are changed implicitly  
 206 using the PREM average within each layer. However, even the largest EL  
 207 variation in our test range (40 km vs 120 km) causes at most only  $|\Delta u| < 5 \mu\text{m}$   
 208 directly along the margins of the ice load (Fig. 4). Everywhere else this effect  
 209 is even smaller such that  $|\Delta u| \ll 1 \mu\text{m}$ . This is  $\ll 1\%$  of the eustatic rate  
 210 of  $\text{WANT}_{\text{el}}$ . Thus, the impact of EL variations - in a reliable range - on uplift  
 211 rates induced by  $\text{WANT}_{\text{el}}$  can be seen as neglectable.

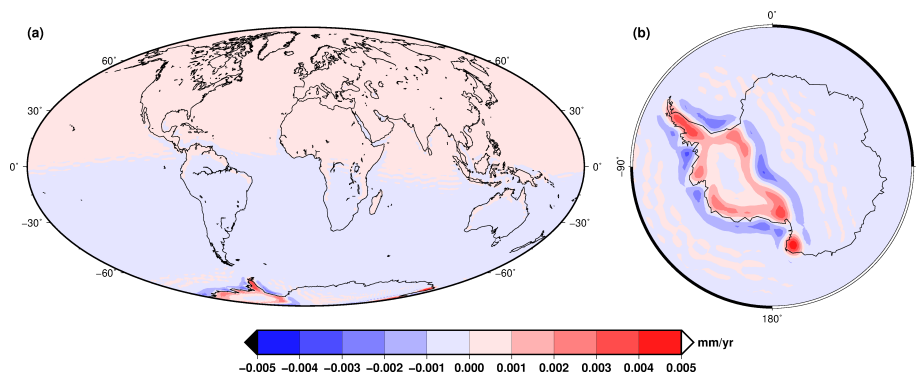


**Figure 4**  
 Difference of the elastic uplift rate from the present-day loading scenario  $\text{WANT}_{\text{el}}$  between  
 an elastic lithosphere of  $d_{\text{EL}} = 120$  km and  $d_{\text{EL}} = 40$  km.



212 *4.2. Impact on the viscous contribution*

213 We test the sensitivity of the viscous contribution by examining the GIA  
214 response to the long-term ice loading scenario ICE-6G. Generally, the viscous  
215 contribution is affected by both EL variations and viscosity variations. We found  
216 that Earth structure variations at great distances show a neglectable mean im-  
217 pact (Eq. 5) on the local uplift rates for both types of variations. We compute  
218 the mean impact of the EL variations (Fig. 5(a),(c)) from the 96 model combi-  
219 nations with the largest EL variation within our test range ( $d_{\text{EL}} = 120$  km vs  
220  $d_{\text{EL}} = 40$  km) in combination with non-varying viscosities  $\mu_{\text{SUM,DUM,TZ}}$ .

221  
222 The mean impact of the viscosity variations (Fig. 5(b),(d)) involves the 1269  
223 model combinations with varying viscosities between the Antarctic and Non-  
224 Antarctic Earth structure based on all 48 viscosity settings in the Antarctic re-  
225 gion and 27 settings in the Non-Antarctic region (excl.  $\mu_{\text{SUM,DUM}} = 10^{18}$  Pa s).  
226 The EL thickness in both Earth structures is held at  $d_{\text{EL}} = 120$  km. Both load  
227 components (ICE-6far, ICE-6ant) show a large mean impact  $\overline{\Delta u} > 0.6 \frac{\text{mm}}{\text{yr}}$   
228 in their local region around their characteristic distribution of the ice load  
229 (Fig. 5(a)-(d), red/black areas), where we account for the variations, but only  
230 a minor impact of  $\overline{\Delta u} < 0.2 \frac{\text{mm}}{\text{yr}}$  (white/yellow areas) in their far-field re-  
231 gion. These mean impacts on uplift rate should be compared to uplift rates of  
232  $u \sim 5 \frac{\text{mm}}{\text{yr}}$ , which is a typical value for the main pattern of uplift in Antarctica  
233 from the ICE-6G(VM5a) loading scenario (Argus et al., 2014).

234  
235 We analyzed in the same manner the mean impact of variations at near  
236 distances via the load components ICE-6eant and ICE-6want (Fig. 5(e)-(h)).  
237 For EL variations, we computed the mean impact of 96 model combinations of  
238 non-varying viscosities, but with an EL variation of  $d_{\text{EL}} = 120$  km vs  $d_{\text{EL}} =$   
239  $60$  km (Fig. 5(e),(f)). Again the EL variations exert a negligible impact on  
240 the uplift rates of the neighboring region. For viscosity variations, the mean  
241 impact is based on the assumption of a stiff East Antarctic Earth structure.  
242 We assume the East Antarctic Earth structure to follow  $W12_{\text{earth}}$ . Thus the  
243 mean impact involves the 47 model combinations with differing viscosities and  
244 an EL thickness of  $d_{\text{EL}} = 120$  km (Fig. 5(g),(h)). The viscosity variations show  
245 a much larger mean impact in the neighboring regions. Especially variations  
246 beneath West Antarctica, which affect the response to ICE-6want, can have  
247 a significant influence in large areas of East Antarctica (Fig. 5(h)). However,  
248 these results (Fig. 5) are based only on the long-term loading of ICE-6G. Next,  
249 we demonstrate how this impact in neighboring regions can decrease if the  
250 considered time period of loading matches the relaxation behavior of the Earth  
251 structure.

252 *4.3. Influence of the time period of loading*

253 Here, we apply the M1DEA to consider the different Earth structures be-  
254 neath East and West Antarctica. East Antarctica uses the stiff Earth structure

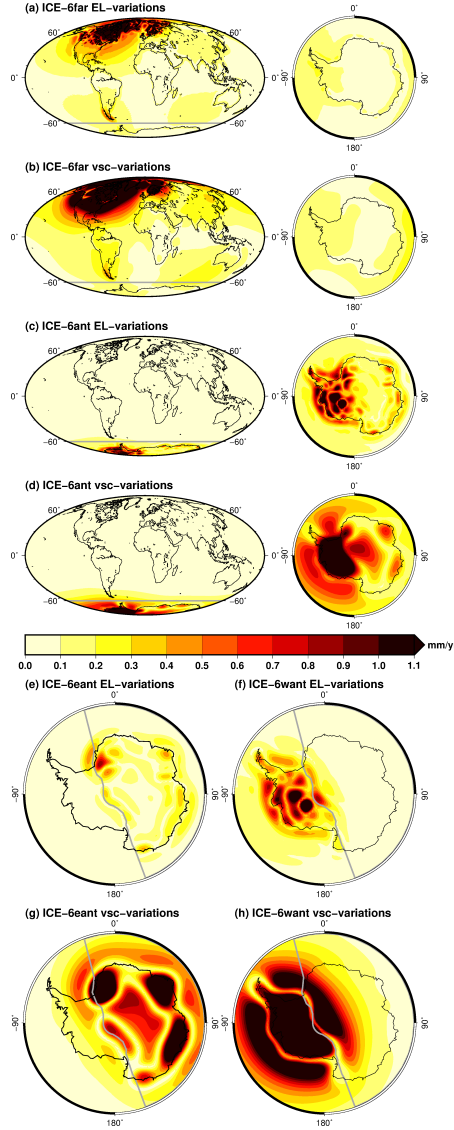


**Figure 5**

Mean impact  $\overline{\Delta u}$  (Eq. 5) of Earth structure variations on present-day GIA uplift rates, for the different components of the ICE-6G loading scenario. The variations shown here should be compared to uplift rates of  $u \approx 5 \frac{\text{mm}}{\text{yr}}$ , which are typical of GIA processes.

**Top:** Mean impact for far-distant variations. (a) EL variations for ICE-6far, (b) viscosity variations for ICE-6far, (c) EL variations for ICE-6ant, (d) viscosity variations for ICE-6ant. The mean impact in (a),(c) comprises  $N_{\text{mod}} = 96$  model combinations using an EL variation of  $d_{\text{EL}} = 120$  km to  $d_{\text{EL}} = 40$  km with non-varying viscosities  $\mu_{\text{SUM,DUM,TZ}}$ . The mean impact in (b),(d) comprises  $N_{\text{mod}} = 1269$  model combinations using a constant EL thickness of  $d_{\text{EL}} = 120$  km with combinatorial varying viscosities  $\mu_{\text{SUM,DUM,TZ}}$  within the test range between local and far-field Earth structure. The gray line in (a)-(d) marks the separation of Antarctic and Non-Antarctic regions.

**Bottom:** Mean impact of near-distant variations. (e) EL variations for ICE-6eant. (f) EL variations for ICE-6want. The mean impact in (e),(f) comprises  $N_{\text{mod}} = 96$  model combinations using an EL variation of  $d_{\text{EL}} = 120$  km to  $d_{\text{EL}} = 60$  km with non-varying viscosities  $\mu_{\text{SUM,DUM,TZ}}$ . (g) viscosity variations for ICE-6eant. (h) viscosity variations for ICE-6want. The mean impact in (g),(h) comprises  $N_{\text{mod}} = 47$  model combinations using a constant EL thickness of  $d_{\text{EL}} = 120$  km, the  $W12_{\text{earth}}$  for East Antarctica and varying viscosities  $\mu_{\text{SUM,DUM,TZ}}$  within the test range for the West Antarctica Earth structure. The gray line in (e)-(h) marks the separation of the East and West Antarctic regions.

255 (W12<sub>earth</sub>, blue line in Fig. 2) while West Antarctica uses the low-viscosity estimate (BAR<sub>earth</sub>, red line in Fig. 2). The present-day uplift rates from only  
256 long-term loads (Fig. 6(a)) show large amplitudes in East Antarctica, where the  
257 GIA is still ongoing due to the slow relaxation of the rigid Earth structure. The  
258 uplift rates in West Antarctica are drastically smaller, since the faster relaxation  
259 of the less viscous Earth causes a nearly finalized GIA. On one hand the impact  
260 of the more rigid East Antarctic Earth structure on the West Antarctic uplift  
261 rates (Eq. 4) results from the "unexpected" slow relaxation of East Antarctica,  
262 but is mostly limited to the margins along the transition of both load components  
263 (Fig. 6(b)). On the other hand the "missing" long-term load signal of the fast  
264 relaxing West Antarctica causes the large impact on neighboring stiff  
265 regions (Fig. 6(c)).  
266

267  
268 In the case of a fast relaxing low-viscosity Earth structure, recent deglaciation  
269 is the major contribution to the present-day uplift rates, as observed if  
270 WANT<sub>100</sub> is included additionally to the loading scenario (Fig. 6(d)). This  
271 leads to an enormous reduction in the differences induced by the less viscous  
272 West Antarctic structure (Fig. 6(f)). The differences mainly follow variations  
273 in the spatial distribution of West Antarctic ice loss between the long-term and  
274 recent loads. The only strong anomaly remaining as impact on the East Antarctic  
275 uplift rates is a tiny belt of subsidence from the collapsing bulges around the  
276 recent load (Fig. 6(f)).  
277

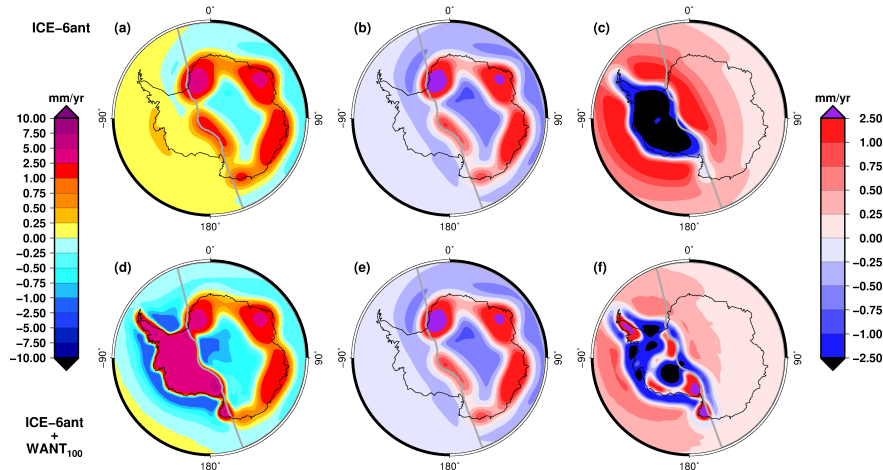


**Figure 6**

MIDEA applied for Antarctic deglaciation using a strong lateral contrast (rigid East Antarctic structure  $W12_{\text{earth}}$ , and super low-viscosity West Antarctic structure  $BAR_{\text{earth}}$ , see Tab. A.3, Fig. 2).

**Top row:** Using only long-term loads of ICE-6G components: (a) Combined uplift rates, (b) Differences  $\Delta u$  (Eq. 4) between the combined and homogeneous uplift rates of the low-viscosity Earth structure, (c) Differences  $\Delta u$  between the combined and homogeneous uplift rates of the rigid Earth structure.

**Bottom row:** Using long-term loads of ICE-6G components and recent load ( $WANT_{100}$ ): (d) Combined uplift rates, (e) Differences  $\Delta u$  between the combined and homogeneous uplift rates of the low-viscosity Earth structure, (f) Differences  $\Delta u$  between the combined and homogeneous uplift rates of the rigid Earth structure. The gray line marks the separation of East and West Antarctica.

278 Alternatively, the W12 ice loading scenario (Whitehouse et al., 2012a,b)  
 279 can be used as a long-term model. Using W12 loading confirms the results  
 280 using ICE-6G (Fig. 5, 6), resulting in similar mean impacts and even smaller  
 281 differences when the recent load is included (see App.: Fig. B.2, B.3).

## 282 5. Assessment of the MIDEA

283 The existing global predictions of SLC and GIA (e.g. ICE-6G(VM5a), Peltier  
 284 et al., 2015), which are based on a classical radially-symmetric Earth structure,  
 285 are not able to explain regionally-observed rapid uplift rates, e.g. in the Amundsen  
 286 Sea Embayment (Barletta et al., 2018). The presented MIDEA and recent  
 287 similar approaches (Khan et al., 2016; Sasgen et al., 2017, 2018) can implement  
 288 a locally-appropriate Earth structure and therefore allow us to consider lateral  
 289 variations in Earth structure. As our sensitivity analysis of the MIDEA (Fig. 5)  
 290 reveals, a considered variation of the Earth structure for a specific load component  
 291 affects mainly the region of the load component itself and a relatively  
 292 narrow region surrounding it. For an ice history involving both long-term and  
 293 recent loading, the MIDEA improves estimates of SLC and GIA in regions with

294 strong viscosity variations compared to using a single 1D Earth structure. Ac-  
295 cording to the analysis of [Paulson et al. \(2005\)](#), displacement rates are strongly  
296 sensitive to the local viscosity structure beneath the load and observation point,  
297 and less related to the global mean structure. This supports the application of  
298 the M1DEA to account for viscosity anomalies below the different load com-  
299 ponents, although the M1DEA cannot consider potential viscosity anomalies  
300 for the observation points. Such a treatment requires a fully 3D finite element  
301 model ([Paulson et al., 2005](#)).

302  
303 Nevertheless, the M1DEA represents a straight-forward approximation to  
304 test the effect of lateral variations in Earth structure. In particular, the com-  
305 bined rates of the M1DEA result from multiple definitions of a globally uniform  
306 relaxation behavior. Thus, they contain contributions from the various different  
307 load components, each modeled with a different and locally-appropriate Earth  
308 structure. By contrast, the globally uniform relaxation behavior of a 1D Earth  
309 structure implies spatially symmetric transmission of stresses and flow patterns  
310 around any load. Using only a single 1D Earth structure, the equal relaxation  
311 behavior compensates the influence of neighboring load components. The su-  
312 perposition of uplift and SLC rates from different uniform relaxation behaviors  
313 interrupts this implicit compensation between neighboring regions.

314  
315 Compared to full 3D finite element/volume solutions any asymmetric trans-  
316 mission of stresses at the margins of the neighboring components is neglected by  
317 the M1DEA ([Khan et al., 2016](#); [Sasgen et al., 2018](#)). The differences between a  
318 full 3D model and M1DEA solutions are thus expected to be largest along the  
319 margins of neighboring regions with different Earth structures. In particular,  
320 peripheral bulges within the M1DEA are predicted from the Earth structure  
321 beneath the corresponding load component, even if the bulge might be located  
322 in a neighboring region with a different Earth structure (Fig. 7). Our sensitivity  
323 analysis (Fig. 5(e)-(h)) clearly reveals this bulge impact in the neighboring re-  
324 gion, and illustrates what may be the largest source of modeling error associated  
325 with the M1DEA. However, our results for Antarctica are consistent with the  
326 recent comparison of a 3D vs 1D Earth structure by [Hay et al. \(2017\)](#), who used  
327 a finite volume model.

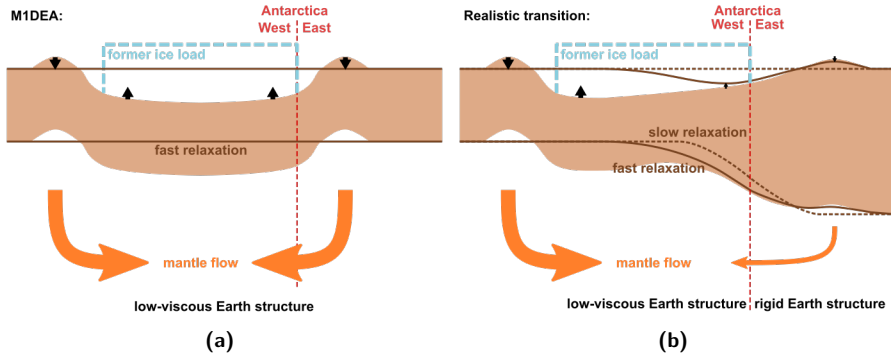


**Figure 7**

Schematic GIA effect for a load (dashed blue) on a low-viscosity Earth structure (like West Antarctica) in the direct vicinity of a transition to a high-viscosity Earth structure (like East Antarctica). The red dashed line marks the border between both regions. The brown area is the initial state of the EL. The solid brown lines mark the state after the full relaxation of the low-viscosity structure. The dashed brown lines show the state after the full relaxation of the high-viscosity structure. The orange arrows indicate the mantle flow, and the black arrows the observed uplift rates during the fast relaxation. (a) The predicted relaxation by the M1DEA assumes a globally West Antarctic structure with a laterally-symmetric relaxation. As the entire load is located on the low-viscosity structure, the bulge in East Antarctica still follows the fast relaxation. The GIA is already finalized after the fast relaxation (solid brown = dashed brown). (b) The relaxation of a realistic transition introduces an asymmetric initial deformation. The low-viscosity side fully relaxes in the first phase with large mantle flow and large uplift rates. The high-viscosity side is characterized by a different initial deformation of longer wavelength and smaller amplitude, and relaxes only slowly with less mantle flow and small uplift rates during the first period of faster relaxation.

328 In the following we discuss the impact of this cross-region effect for the  
 329 different parameters of the Earth structure and different aspects of M1DEA  
 330 solutions, and how it can be minimized.

331 *5.1. Modeling variations in elastic lithosphere*

332 In general, the influence of the EL thickness on present-day uplift rates be-  
 333 comes apparent in small-scale variations of the viscous (postglacial) response.  
 334 These variations mainly affect the short wavelength patterns of uplift rates re-  
 335 lated to small-scale structures of the chosen loading scenario. A thinner EL  
 336 increases the amplitudes and shortens the wavelength of the predicted uplift  
 337 rates, compared to the thicker EL. This behavior is also demonstrated by the  
 338 3D approach of Nield et al. (2018). The mean impact  $\overline{\Delta u}$  (Eq. 5) from EL vari-  
 339 ations is strongly limited to each region and shows only neglectable effects on  
 340 other regions (far-distant and near-distant, Fig. 5(a),(c),(e),(f)). This indicates  
 341 reasonable results for the M1DEA when considering EL variations in the pre-  
 342 dictions of viscous uplift rates, despite the neglected asymmetric transmission  
 343 of stresses.

344

345 The elastic response of the Earth shows a neglectable sensitivity to strong  
346 variations of the EL thickness (Fig. 4). Consequently, no significant accuracy is  
347 gained, but also no bias is introduced, by the M1DEA in the predicted elastic  
348 contribution. This enhances the findings of [Mitrovica et al. \(2011\)](#), and confirms  
349 the typical fingerprint character of the elastic contribution mainly determined  
350 by the location and amount of (ice or water) load.

### 351 5.2. Modeling variations in upper mantle viscosities

352 Laterally-varying upper mantle viscosities affect the entire large-scale uplift  
353 pattern including both the region of ice loading and the surrounding bulges  
354 in the near-field of the local ice load. Hence, the mean impact  $\overline{\Delta u}$  (Eq. 5) of  
355 viscosity variations beneath near-distant and neighboring loads shows a poten-  
356 tially large influence on the local rates (Fig. 5(g),(h)), whereas the effect of a  
357 viscosity variation beneath a far-distant load remains locally still neglectable  
358 (Fig. 5(b),(d)).

359 Strong contrasts of the upper mantle viscosities between neighboring regions  
360 cause large differences in their time scales of relaxation. High viscosities lead to  
361 a slow relaxation with present-day rates most sensitive to ice loading at 1 to 100  
362 kyr before present, whereas low viscosities result in a much faster relaxation,  
363 with the highest amplification resulting from ice loading that happened decades  
364 or centuries ago. For the M1DEA, this results in two magnifying effects: First,  
365 the stronger contrasts result in larger differences in rates between regions due to  
366 inhomogeneous compensation of bulges from connected loads. Second, the fast  
367 relaxation for low-viscosity Earth structures can diminish the local contribution  
368 to the rates obtained from long-term loading scenarios (Fig. 6(a)). Both yield  
369 large impacts  $\Delta u$  (Eq. 4) on local uplift rates along the margins of neighboring  
370 load components with strong viscosity contrasts between them (Fig. 6(a)-(c)),  
371 according to the general discussion above.

372  
373  
374 We clearly demonstrate that the inclusion of a recent ice load in a region  
375 of fast relaxation can drastically reduce the specific impact  $\Delta u$  (Eq. 4) of the  
376 low-viscosity region on neighboring regions (Fig. 6(d)-(f)), in particular if recent  
377 and long-term loading act in parallel (e.g. ice loss for both). The recent ice loss  
378 introduces an additional contribution, which recovers the dominance of the con-  
379 tribution from the local load component in the local rates (compare the West  
380 Antarctic region in Fig. 6(d) vs Fig. 6(a)). Further, the rapid response to the  
381 recent ice loss compensates the missing counterpart of the peripheral bulge at  
382 the margins of neighboring deglaciating regions, which mimics to some degree  
383 the behavior of a 3D Earth structure as observed in [Hay et al. \(2017\)](#). De-  
384 pending on the recent ice change, this effect will be largest for strong contrasts  
385 that include very low viscosities. How accurately this synthetic combination  
386 embodies the actual 3D effects at the margins cannot be explicitly clarified in  
387 this paper and must be tested against a full 3D finite element approach using  
388 various lateral Earth structure variations for a range of grid resolutions and

389 maximum spherical degrees, respectively.

390

391 Any type of modeling that includes lateral variations of upper mantle vis-  
392 cosities requires regional components that deglaciate at the time scales of their  
393 regional relaxation. Thus, the M1DEA provides a computationally cheap way  
394 to assess the effect of even strong lateral variations of upper mantle viscosity  
395 between large-scale load components.

### 396 *5.3. Modeling with large-scale and small-scale components*

397 Assuming the same arbitrary Earth structure, a large-scale load is associated  
398 with stronger bulges of longer wavelength than a small-scale load. Consequently,  
399 large-scale loads have a bigger bulge impact  $\Delta u$  (Eq. 4) on the rates in the  
400 neighboring region. Also, a strong contrast in the Earth structure between  
401 neighboring load components leads to a broader bulge impact along the Earth  
402 structure variation. Introducing more small-scale components in the vicinity of  
403 a strongly varying Earth structure (e.g. the Trans Antarctic mountains) allows  
404 M1DEA to address variations in Earth structure more continuously with smaller  
405 contrasts. This should significantly reduce the big bulge impacts in such regions,  
406 since:

- 407 • The smaller contrasts may introduce bulges that better compensate each  
408 other, like uniform structures would do.
- 409 • Smaller scale load components affect narrower margins along the transi-  
410 tion.

411 The tests in this paper are based on large-scale components with relatively  
412 strong contrasts between their Earth structures and do not include a small-  
413 scale load transition. Therefore, the obtained differences should define an upper  
414 limit for the amplitude and wavelength of the bulge impact of the neighbor-  
415 ing Earth structure along the margin. Nevertheless, these models already show  
416 differences, which justify the application of the M1DEA. Thus with the ad-  
417 dition of a small-scale load transition, the M1DEA would seem to offer great  
418 capabilities to model GIA and SLC for lateral variations in Earth structure for  
419 relatively small computational cost. Recent GIA models for Greenland (Khan  
420 et al., 2016) and Antarctica (Sasgen et al., 2017, 2018) have already started to  
421 use the M1DEA with small-scale components. However, it cannot completely  
422 be ruled out that very large contrasts on a small scale within the 3D Earth  
423 structure may compromise the accuracy of the M1DEA. Here as well, further  
424 tests against fully 3D finite element models are needed to investigate the accu-  
425 racy of the M1DEA along the transition between neighboring Earth structures  
426 for continuous variations with small-scale load components. These tests should  
427 consider many parameters for both approaches, e.g. the grid resolution of the  
428 finite element model, the maximum spherical harmonic degree of the M1DEA,  
429 the number and size of load components in the M1DEA, in order to compare  
430 both approaches in accuracy and computation time.



#### 431 5.4. Modeling rotational feedback

432 Above we discussed the possible local artifacts of the M1DEA that are di-  
433 rectly linked to the margins of neighboring load components. These are of  
434 course the most obvious uncertainties. Beside these local effects, SLC and GIA  
435 also include global features that are mainly decoupled from the load location,  
436 e.g. the RFB. The RFB always appears with a spherical harmonic (2,1)-pattern  
437 varying in amplitude depending on load amount, load position, loading time,  
438 and the Earth structure. The M1DEA simply combines classical 1D SLE so-  
439 lutions for multiple load components with global 1D Earth structures, which  
440 are locally-appropriate (Eq. 3). Thus, the RFB contribution of each solution  
441 assumes the locally-appropriate Earth structure to be globally valid. Conse-  
442 quently, we cannot rule out that including RFB within the M1DEA might over-  
443 or underestimate the RFB contribution of some load components compared to  
444 the real 3D rheology structure of the entire Earth, which can affect coupling to  
445 other harmonics on a self-gravitationally consistent Earth (Paulson et al., 2005).

446 To deal with this problem following the idea of the M1DEA, we suggest  
447 that either an estimate of the total RFB by a mean Earth structure (i.e., less  
448 M1DEA) or a separate modeling of the ocean load of each component with  
449 a consistent oceanic Earth structure (i.e., even more M1DEA!) can reduce this  
450 uncertainty and increase the accuracy of the estimated total RFB. However, our  
451 calculations show that the Antarctic load components induce too little viscous  
452 RFB - most probably due to their location too close to the South pole - to  
453 satisfy a detailed analysis of the RFB approximation within the M1DEA that  
454 would be comparable to the treatment by Paulson et al. (2005).

## 456 6. Conclusions

457 We tested a new approach for using the pseudo-spectral form of the sea level  
458 equation (SLE) to account for lateral variations in Earth structure, namely  
459 upper mantle viscosities and elastic thickness of the lithosphere. This Multi-  
460 ple 1D Earth Approach (M1DEA) predicts global sea level change (SLC) and  
461 ground uplift rates using the superposition of separately calculated solutions of  
462 the pseudo-spectral SLE for each regional component of the ice load. Lateral  
463 heterogeneity in Earth structure is accommodated in M1DEA by utilizing differ-  
464 ent, locally-appropriate, 1D Earth structures for each individual solution. Our  
465 analysis of the sensitivity of local uplift rates to variations in Earth structure  
466 suggests:

- 467 1. The elastic contribution of SLC and uplift rates is (nearly) independent  
468 from Earth structure variations. Therefore, the M1DEA is applicable  
469 without any bias, but also without much benefit, for the predictions of  
470 elastic sea level fingerprints.
- 471 2. The viscous contribution is strongly affected by Earth structure variations.  
472 However, the effect of variations in elastic thickness of the lithosphere is

473 locally limited, meaning that the M1DEA can usefully account for such  
474 variations.

475 3. The viscous contribution to SLC and uplift rates depends on the local  
476 viscosity structure but also to some degree on the viscous structure of  
477 neighboring regions. This inability to adequately handle peripheral bulges  
478 that extend into neighboring regions with differing viscosity structures is a  
479 limitation of the M1DEA. However, the M1DEA can account for viscosity  
480 variations if:

481 a) Each regional load component includes deglaciation associated with  
482 its individual time scale of relaxation, i.e. short-timescale loads are  
483 present in fast-relaxing regions (such as West Antarctica), and longer-  
484 timescale loads are present in more slowly relaxing regions (such as  
485 East Antarctica).

486 b) The load is subdivided into small-scale components in areas of strong  
487 variations, in order to maintain small viscosity contrasts between  
488 neighboring Earth structures.

489 In summary, our sensitivity analysis of the M1DEA for the pseudo-spectral  
490 SLE demonstrates the potential in its application. Further tests should compare  
491 predictions from M1DEA models directly against 3D finite element models  
492 (3D FEM) to characterize the relative accuracy of the M1DEA (in particular  
493 regarding recommendation 3.b), and the benefit in terms of computation time,  
494 with respect to the grid resolution (3D FEM), the maximum spherical harmonic  
495 degree (M1DEA), and the number of load components (M1DEA). A sophisticated  
496 M1DEA can potentially contribute usefully to more accurate predictions  
497 of GIA-inferred uplift rates at reduced computational cost. Such predictions  
498 are essential for enhancing models of Antarctic ice history, estimates of recently  
499 accelerated present-day Antarctic ice loss, and the probability for a future col-  
500 lapse or stability of Antarctic ice sheets. In the future, coupled climate models  
501 will hopefully benefit from these improvements.

## 502 **Acknowledgments**

503 We thank the editor, Irina Artemieva, and two anonymous reviewers for  
504 their critical feedback, which helped to improve the manuscript. Furthermore,  
505 we thank Pippa Whitehouse for her kind cooperation in providing her ice model  
506 and the following discussion, which clarified issues related to ESL and the im-  
507 portant difference between total and effective ice thickness. This work was  
508 supported partly by the Research Council of Norway's projects 223272 (Centre  
509 of Excellence) and 288449 (CPC).

## 510 **References**

511 Amante, C. and Eakins, B. (2009). Etopo1 1 arc-minute global relief model: Pro-  
512 cedures, data sources and analysis. Technical report, NOAA Technical Mem-  
513 orandum NESDIS NGDC-24. National Geophysical Data Center, NOAA.

- 514 An, M., Wiens, D. A., Zhao, Y., Feng, M., Nyblade, A. A., Kanao, M.,  
515 Li, Y., Maggi, A., and Lvque, J.-J. (2015). S-velocity model and inferred  
516 Moho topography beneath the Antarctic Plate from Rayleigh waves: Antarc-  
517 tic S-velocities and Moho. Journal of Geophysical Research: Solid Earth,  
518 120(1):359–383.
- 519 Argus, D. F., Peltier, W. R., Drummond, R., and Moore, A. W. (2014). The  
520 Antarctica component of postglacial rebound model ICE-6g\_c (VM5a) based  
521 on GPS positioning, exposure age dating of ice thicknesses, and relative sea  
522 level histories. Geophysical Journal International, 198(1):537–563.
- 523 Barletta, V. R., Bevis, M., Smith, B. E., Wilson, T., Brown, A., Bordoni,  
524 A., Willis, M., Khan, S. A., Rovira-Navarro, M., Dalziel, I., Smalley, R.,  
525 Kendrick, E., Konfal, S., Caccamise, D. J., Aster, R. C., Nyblade, A., and  
526 Wiens, D. A. (2018). Observed rapid bedrock uplift in Amundsen Sea Em-  
527 bayment promotes ice-sheet stability. Science, 360(6395):1335–1339.
- 528 Chen, J. L., Wilson, C. R., Blankenship, D., and Tapley, B. D. (2009). Ac-  
529 celerated Antarctic ice loss from satellite gravity measurements. Nature  
530 Geoscience, 2(12):859–862.
- 531 Dziewonski, A. M. and Anderson, D. L. (1981). Preliminary reference earth  
532 model. Physics of the Earth and Planetary Interiors, 25(4):297 – 356.
- 533 Farrell, W. E. and Clark, J. A. (1976). On Postglacial Sea Level. Geophysical  
534 Journal of the Royal Astronomical Society, 46(3):647–667.
- 535 Fretwell, P., Pritchard, H. D., Vaughan, D. G., Bamber, J. L., Barrand, N. E.,  
536 Bell, R., Bianchi, C., Bingham, R. G., Blankenship, D. D., Casassa, G.,  
537 Catania, G., Callens, D., Conway, H., Cook, A. J., Corr, H. F. J., Damaske,  
538 D., Damm, V., Ferraccioli, F., Forsberg, R., Fujita, S., Gim, Y., Gogineni,  
539 P., Griggs, J. A., Hindmarsh, R. C. A., Holmlund, P., Holt, J. W., Jacobel,  
540 R. W., Jenkins, A., Jokat, W., Jordan, T., King, E. C., Kohler, J., Krabill, W.,  
541 Riger-Kusk, M., Langley, K. A., Leitchenkov, G., Leuschen, C., Luyendyk,  
542 B. P., Matsuoka, K., Mouginot, J., Nitsche, F. O., Nogi, Y., Nost, O. A.,  
543 Popov, S. V., Rignot, E., Rippin, D. M., Rivera, A., Roberts, J., Ross, N.,  
544 Siegert, M. J., Smith, A. M., Steinhage, D., Studinger, M., Sun, B., Tinto,  
545 B. K., Welch, B. C., Wilson, D., Young, D. A., Xiangbin, C., and Zirizzotti,  
546 A. (2013). Bedmap2: improved ice bed, surface and thickness datasets for  
547 Antarctica. The Cryosphere, 7(1):375–393.
- 548 Harley, S. L., Fitzsimons, I. C. W., and Zhao, Y. (2013). Antarctica and super-  
549 continent evolution: historical perspectives, recent advances and unresolved  
550 issues. Geological Society, London, Special Publications, 383(1):1–34.
- 551 Hay, C. C., Lau, H. C. P., Gomez, N., Austermann, J., Powell, E., Mitrovica,  
552 J. X., Latychev, K., and Wiens, D. A. (2017). Sea Level Fingerprints in a  
553 Region of Complex Earth Structure: The Case of WAIS. Journal of Climate,  
554 30(6):1881–1892.

- 555 Jacob, T., Wahr, J., Pfeffer, W. T., and Swenson, S. (2012). Recent contribu-  
556 tions of glaciers and ice caps to sea level rise. Nature, 482(7386):514–518.
- 557 Kendall, R. A., Mitrovica, J. X., and Milne, G. A. (2005). On post-glacial  
558 sea level - II. Numerical formulation and comparative results on spherically  
559 symmetric models. Geophysical Journal International, 161(3):679–706.
- 560 Khan, S. A., Sasgen, I., Bevis, M., van Dam, T., Bamber, J. L., Wahr, J., Willis,  
561 M., Kjær, K. H., Wouters, B., Helm, V., Csatho, B., Fleming, K., Bjrck, A. A.,  
562 Aschwanden, A., Knudsen, P., and Munneke, P. K. (2016). Geodetic measure-  
563 ments reveal similarities between post-Last Glacial Maximum and present-day  
564 mass loss from the Greenland ice sheet. Science Advances, 2(9):e1600931.
- 565 Martin-Español, A., King, M. A., Zammit-Mangion, A., Andrews, S. B., Moore,  
566 P., and Bamber, J. L. (2016). An assessment of forward and inverse GIA  
567 solutions for Antarctica. Journal of Geophysical Research: Solid Earth,  
568 121(9):6947–6965.
- 569 Milne, G. A. and Mitrovica, J. X. (1998). Postglacial sea-level change on a  
570 rotating Earth. Geophysical Journal International, 133(1):1–19.
- 571 Milne, G. A., Mitrovica, J. X., and Davis, J. L. (1999). Near-field hydro-  
572 isostasy: the implementation of a revised sea-level equation. Geophysical  
573 Journal International, 139:464–482.
- 574 Mitrovica, J. X., Gomez, N., Morrow, E., Hay, C., Latychev, K., and Tamisiea,  
575 M. E. (2011). On the robustness of predictions of sea level fingerprints:  
576 On predictions of sea-level fingerprints. Geophysical Journal International,  
577 187(2):729–742.
- 578 Mitrovica, J. X., Milne, G. A., and Davis, J. L. (2001). Glacial isostatic adjust-  
579 ment on a rotating earth. Geophysical Journal International, 147(3):562–578.
- 580 Mitrovica, J. X. and Peltier, W. R. (1991). On postglacial geoid subsidence  
581 over the equatorial oceans. Journal of Geophysical Research: Solid Earth,  
582 96(B12):20053–20071.
- 583 Mitrovica, J. X., Wahr, J., Matsuyama, I., and Paulson, A. (2005). The ro-  
584 tational stability of an ice-age earth. Geophysical Journal International,  
585 161(2):491–506.
- 586 Munk, W. H. and MacDonald, G. J. (1960). The Rotation of the Earth: A  
587 Geophysical Discussion, 323 pp. Cambridge Univ. Press, New York.
- 588 Nield, G. A., Barletta, V. R., Bordoni, A., King, M. A., Whitehouse, P. L.,  
589 Clarke, P. J., Domack, E., Scambos, T. A., and Berthier, E. (2014). Rapid  
590 bedrock uplift in the Antarctic Peninsula explained by viscoelastic response  
591 to recent ice unloading. Earth and Planetary Science Letters, 397:32–41.

- 592 Nield, G. A., Whitehouse, P. L., vanderWal, W., Blank, B., O'Donnell, J. P.,  
593 and Stuart, G. W. (2018). The impact of lateral variations in lithospheric  
594 thickness on glacial isostatic adjustment in West Antarctica. Geophysical  
595 Journal International, 214(2):811–824.
- 596 Paulson, A., Zhong, S., and Wahr, J. (2005). Modelling post-glacial re-  
597 bound with lateral viscosity variations. Geophysical Journal International,  
598 163(1):357–371.
- 599 Peltier, W. R., Argus, D. F., and Drummond, R. (2015). Space geodesy con-  
600 strains ice age terminal deglaciation: The global ICE-6g\_c (VM5a) model:  
601 Global Glacial Isostatic Adjustment. Journal of Geophysical Research: Solid  
602 Earth, 120(1):450–487.
- 603 Peltier, W. R. and Drummond, R. (2008). Rheological stratification of the litho-  
604 sphere: A direct inference based upon the geodetically observed pattern of  
605 the glacial isostatic adjustment of the North American continent. Geophysical  
606 Research Letters, 35(16).
- 607 Rignot, E., Bamber, J. L., van den Broeke, M. R., Davis, C., Li, Y., van de  
608 Berg, W. J., and van Meijgaard, E. (2008). Recent Antarctic ice mass loss  
609 from radar interferometry and regional climate modelling. Nature Geoscience,  
610 1(2):106–110.
- 611 Sasgen, I., Martn-Español, A., Horvath, A., Klemann, V., Petrie, E. J., Wouters,  
612 B., Horvath, M., Pail, R., Bamber, J. L., Clarke, P. J., Konrad, H., and  
613 Drinkwater, M. R. (2017). Joint inversion estimate of regional glacial isostatic  
614 adjustment in Antarctica considering a lateral varying Earth structure (ESA  
615 STSE Project REGINA). Geophysical Journal International, 211(3):1534–  
616 1553.
- 617 Sasgen, I., Martn-Español, A., Horvath, A., Klemann, V., Petrie, E. J., Wouters,  
618 B., Horvath, M., Pail, R., Bamber, J. L., Clarke, P. J., Konrad, H., Wil-  
619 son, T., and Drinkwater, M. R. (2018). Altimetry, gravimetry, GPS and  
620 viscoelastic modeling data for the joint inversion for glacial isostatic adjust-  
621 ment in Antarctica (ESA STSE Project REGINA). Earth System Science  
622 Data, 10(1):493–523.
- 623 Spada, G., Melini, D., and Colleoni, F. (2015). Selen v2.9.12 [software].
- 624 Spada, G., Melini, D., Galassi, G., and Colleoni, F. (2012). Modeling sea level  
625 changes and geodetic variations by glacial isostasy: the improved SELEN  
626 code. [arXiv:1212.5061](https://arxiv.org/abs/1212.5061) [physics]. arXiv: 1212.5061.
- 627 Spada, G. and Stocchi, P. (2007). SELEN: A Fortran 90 program for solving  
628 the "sea-level equation". Computers & Geosciences, 33(4):538–562.
- 629 The IMBIE team (2018). Mass balance of the Antarctic Ice Sheet from 1992 to  
630 2017. Nature, 558(7709):219–222.

- 631 van der Wal, W., Whitehouse, P. L., and Schrama, E. J. (2015). Effect of  
632 GIA models with 3d composite mantle viscosity on GRACE mass balance  
633 estimates for Antarctica. Earth and Planetary Science Letters, 414:134–143.
- 634 Whitehouse, P. L., Bentley, M. J., and Le Brocq, A. M. (2012a). A deglacial  
635 model for Antarctica: geological constraints and glaciological modelling as a  
636 basis for a new model of Antarctic glacial isostatic adjustment. Quaternary  
637 Science Reviews, 32:1–24.
- 638 Whitehouse, P. L., Bentley, M. J., Milne, G. A., King, M. A., and Thomas,  
639 I. D. (2012b). A new glacial isostatic adjustment model for Antarctica: cali-  
640 brated and tested using observations of relative sea-level change and present-  
641 day uplift rates: A new GIA model for Antarctica. Geophysical Journal  
642 International, 190(3):1464–1482.
- 643 Zhao, C., King, M. A., Watson, C. S., Barletta, V. R., Bordoni, A., Dell, M.,  
644 and Whitehouse, P. L. (2017). Rapid ice unloading in the Fleming Glacier  
645 region, southern Antarctic Peninsula, and its effect on bedrock uplift rates.  
646 Earth and Planetary Science Letters, 473:164–176.

647 **Appendix A. Data and setup details**

**Table A.1**

Numerical setup of *SELEN* used for all calculations of the SLE in this publication.

Parameter	Description	Value
$l_{\max}$	Max. spherical harmonic degree	128
$N_{\text{it}}$	Number of iterations	3
$R$	Grid resolution parameter	44
$N_p$	Number of global pixels	75692
	Degree $l = 1$ Love numbers	Included
	Reference frame	Center of mass

**Table A.2**

Summary of the layers and their general parameters for all Earth structures in this publication. The star \* indicates values that are PREM-averaged within the different layers. Hence, the density and shear moduli of EL and SUM depend on the chosen thickness  $d_{\text{EL}} \in [40 \text{ km}, 120 \text{ km}]$ , but are still PREM averaged. var marks an arbitrary variable.

Layer	Basal depth $d$ [km]	Density $\rho$ [ $\frac{\text{kg}}{\text{m}^3}$ ]	Shear modulus $G$ [ $10^{11}$ Pa]	Viscosity $\mu$
EL	[40, 120]	*	*	elastic
SUM	220	*	*	var
DUM	400	3475.5*	0.7649*	var
TZ	670	3857.7*	1.0648*	var
LM	2891	4877.9*	2.1948*	var
Core	6371	10931.7*	0	0

**Table A.3**

Summary of the variable parameters for the Earth structures in this publication:  $d_{\text{EL}}$  is the thickness of the EL.  $\mu_{\text{SUM}, \text{DUM}, \text{TZ}, \text{LM}}$  are the viscosities in the four mantle layers SUM, DUM, TZ, and LM. Within the test range the parameters can be any of the distinct multiple values for each layer. All structures use a lower mantle viscosity of  $\mu_{\text{LM}} = 10^{21.5}$  Pa s.

Structure	$d_{\text{EL}}$ [km]	$\mu_{\text{SUM}}$ [	$\mu_{\text{DUM}}$ $\log_{10}$ Pa s	$\mu_{\text{TZ}}$	$\mu_{\text{LM}}$ ]
W12 <sub>earth</sub>	120	21	21	21	21.5
BAR <sub>earth</sub>	60	18.6	19.2	19.4	21.5
Test range	{40, 60, 90, 120}	{18, 19, 20, 21}	{18, 19, 20, 21}	{19, 20, 21}	21.5

648 The effective ice load  $I_i(\vartheta, \varphi)$  at each location  $(\vartheta, \varphi)$  and time step  $i$ , i.e. the  
649 ice above neutral buoyancy, is estimated from the original total ice thickness  
650  $I_{i,\text{tot}}(\vartheta, \varphi)$  using the present-day bathymetry  $Z(\vartheta, \varphi)$  (Fig. A.1) via:

$$I_i(\vartheta, \varphi) = \begin{cases} I_{i,\text{tot}}(\vartheta, \varphi) & : Z(\vartheta, \varphi) > 0 \\ I_{i,\text{tot}}(\vartheta, \varphi) + \frac{\rho_w}{\rho_{\text{ice}}} Z(\vartheta, \varphi) & : Z(\vartheta, \varphi) < 0, \quad I_{i,\text{tot}}(\vartheta, \varphi) > \left| \frac{\rho_w}{\rho_{\text{ice}}} Z(\vartheta, \varphi) \right| \\ 0 & : Z(\vartheta, \varphi) < 0, \quad I_{i,\text{tot}}(\vartheta, \varphi) \leq \left| \frac{\rho_w}{\rho_{\text{ice}}} Z(\vartheta, \varphi) \right| \end{cases} \quad (\text{A.1})$$

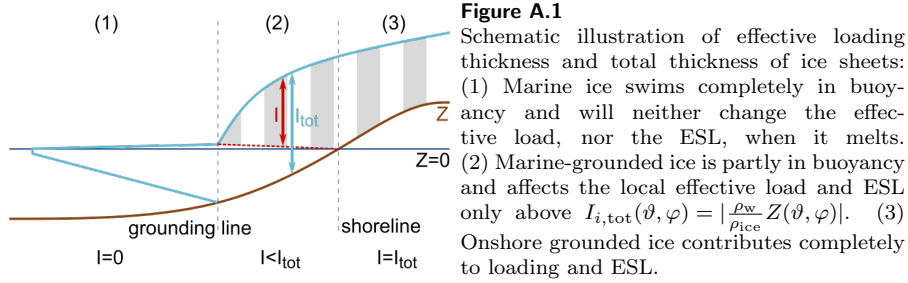


**Table A.4**

Ice loading scenarios used in this publication and their characteristic parameters: The ESL contribution refers to the change after the LGM until now. The temporal discretization  $\Delta t_{\text{Deglac, Glac}}$  for the deglaciation/glaciation period considers ice changes after/before the LGM. The spatial grid resolution  $\Delta\vartheta$  and  $\Delta\varphi$  is uniform in longitudinal and latitudinal direction. The selected bathymetry data set is used for the approximation of the effective ice load of the original ICE-6G files (<http://www.atmosph.physics.utoronto.ca/~peltier/data.php>, downloaded 06.06.2018).

Component	ESL [m]	$\Delta t_{\text{Deglac}}$ [kyr]	$\Delta t_{\text{Glac}}$ [kyr]	$\Delta\vartheta, \Delta\varphi$	Bathymetry
ICE-6far	113.86				ETOPO
ICE-6ant	11.69				BEDMAP2
ICE-6eant	3.88	0.5	2.0	1°	BEDMAP2
ICE-6want	7.81				BEDMAP2
WANT <sub>e1</sub>	$4.6 \cdot 10^{-4}$	0.001	-	0.5°	-
WANT <sub>100</sub>	$4.6 \cdot 10^{-2}$	0.01	-	0.5°	-

## 651 Appendix B. Supporting results

652 *To Figure B.1.:*

653 In previous tests we have analyzed the uplift rates in the Antarctic region and  
654 outside Antarctica. These tests motivated the MIDEA and the sensitivity analysis  
655 presented in this paper.

656

657 In these tests we solved the SLE for each load component (ICE-6far, ICE-  
658 6ant, W12) for all 192 Earth structures. The difference between the rotating  
659 and the non-rotating solutions yields the RFB contribution for each combina-  
660 tion of load component and Earth structure. For comparison, we calculated the  
661  $L_2$ -norm of uplift rates within the region Reg:  $\|\vec{u}_{\text{Reg}}\|_2 = \sqrt{\sum_p u_p^2} \quad \forall p \in \text{Reg}$ ,  
662 where the rates  $u_p$  are computed at pixels  $p$  within the region Reg. Gathering  
663 the values of this regional  $L_2$ -norm depending on the observed region, the ap-  
664 plied load component, and the non-rotating and RFB contributions, yields 12  
665 distributions of  $L_2$ -norms each with a sample size of  $N = 192$  (Fig. B.1).

666



667 It can be observed that uplift rates are dominated by their local component  
 668 of ice loss - (nearly) independently of the Earth structure (Fig.B.1(a) 1st panel,  
 669 (b) 2nd panel). This supports our initial assumption for the M1DEA (Fig. 1).  
 670 Furthermore, Antarctic long-term ice loss is not able to induce a significant  
 671 RFB contribution to the total rates in any component on a postglacial time  
 672 scale ( $\approx 1\%$ ) (Fig.B.1 4th panel).

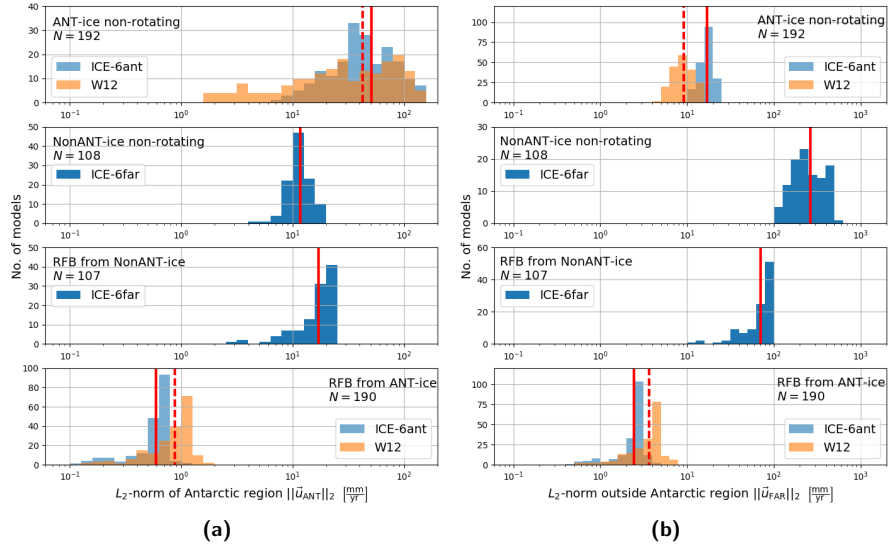


**Figure B.1**  
 Regional average uplift rates in (a) the Antarctic region (south of  $60^\circ S$ ), and (b) the Non-Antarctic region (north of  $60^\circ S$ ). Each panel shows the distribution of the regional average uplift rate for the 192 tested Earth structures for a specific load contribution. The four panels from top to bottom show the contributions from the Antarctic ice load on a non-rotating Earth, the Non-Antarctic ice load on a non-rotating Earth, the RFB induced by the Non-Antarctic ice load, and the RFB induced by the Antarctic ice load. Each value in the different distributions represents the regional  $L_2$ -norm of uplift rates of one load-Earth-combination. The red lines mark the mean values of the distributions for each contributor (red solid: ICE-6 components, red dashed: W12 component).

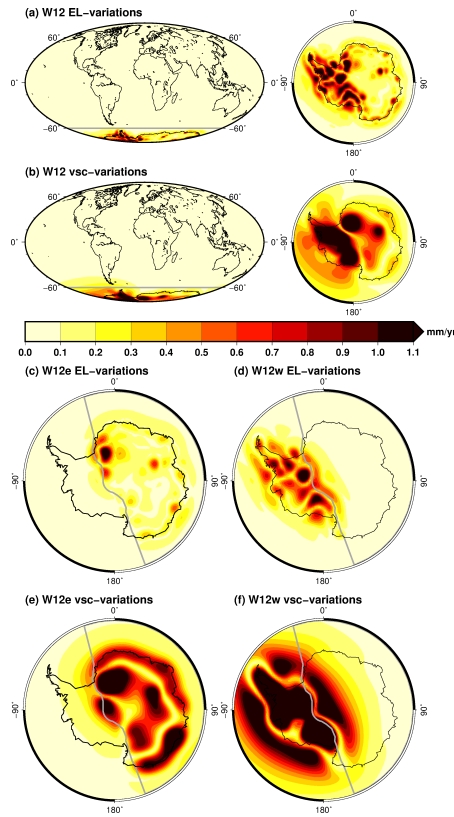


**Figure B.2**

Mean impact  $\overline{\Delta u}$  (Eq. 5) of Earth structure variations on present-day GIA uplift rates, for the different components of the W12 loading scenario. See Fig. 5, which shows the same analysis for the ICE-6G loading scenario, for an explanation of the figure.

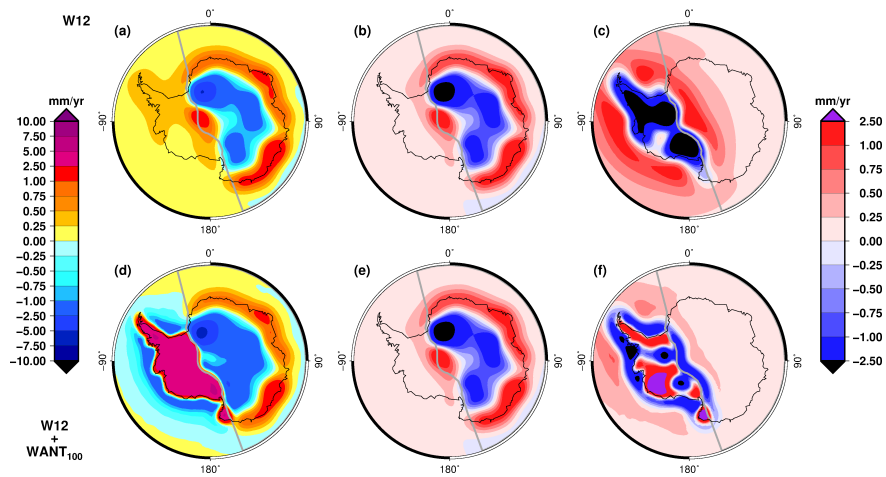


**Figure B.3**

Similar to Fig.6 of the main text, but using W12 ice loads instead of ICE-6G.

673 **Appendix C. Implementation of rotational feedback in *SELEN***

674 The repository [https://github.com/r-hartmann/RFBupdate\\_for\\_SELEN/](https://github.com/r-hartmann/RFBupdate_for_SELEN/)  
675 provides:

- 676 • All subprograms (modified and new) that are required to include the RFB  
677 option in *SELEN* 2.9.12
- 678 • An installation guide
- 679 • Implementation details
- 680 • Theoretical background of the calculation scheme for RFB